


Generalized Hong-Ou-Mandel quantum interference with phase-randomized weak coherent statesYu-Zhe Zhang ^{1,2} Kejin Wei,^{1,2,3} and Feihu Xu^{1,2,*}¹*National Laboratory for Physical Sciences at Microscale and Department of Modern Physics, University of Science and Technology of China, Hefei 230026, China*²*Shanghai Branch, CAS Center for Excellence and Synergetic Innovation Center in Quantum Information and Quantum Physics, University of Science and Technology of China, Shanghai 201315, People's Republic of China*³*Guangxi Key Laboratory for Relativistic Astrophysics, School of Physics Science and Technology, Guangxi University, Nanning 530004, China*

(Received 11 November 2019; accepted 13 February 2020; published 16 March 2020)

In the context of Fock states, demonstrating multiphoton quantum interference, e.g., the generalized Hong-Ou-Mandel (HOM) interference, is at the core of many applications of quantum technologies. However, it is difficult to demonstrate high-visibility quantum interference for a large number of photons. Here, we introduce an experimentally feasible proposal to achieve this goal using phase-randomized weak coherent states and practical photon-number-resolving detectors. Our method can be used to obtain analytically tight bounds of the generalized HOM dip in a beam splitter, and it is robust against practical errors. The simulation shows that for an ideal detector that can resolve any number of photons without an upper bound, the proposed method can bound the generalized HOM interference for a large number of photons, e.g., 100 photons; for a practical detector that can resolve up to 29 photons, the proposed method can bound the generalized HOM interference for 56 photons with visibility 99.4%. Our proposal is a general approach for multiphoton quantum interference in optical networks with multiple inputs and outputs.

DOI: [10.1103/PhysRevA.101.033823](https://doi.org/10.1103/PhysRevA.101.033823)**I. INTRODUCTION**

Multiphoton quantum interference (MQI), in the context of Fock state interference, is a fundamental phenomenon of quantum mechanics. It has fascinated many scientists, as its essential role is showing the difference between quantum physics and classical physics. Over the past decades, MQI has been widely studied in theory and demonstrated in experiments involving two or more photons. MQI is a promising technology to generate NOON states [1] and W states [2], implement $N \times N$ unitaries [3], and to reduce the complexity of photonic quantum circuits [4]. Furthermore, MQI has also many other potential applications, such as quantum computing [5,6], quantum communications [7], boson sampling [8–12], quantum metrology [13–16], and so forth. The phase-randomized weak coherent states are key resources for several applications, such as characterizing multimode linear-optical networks [17] and realizing important quantum communication protocols [18–20].

Among MQI, the seminal two-photon interference at a 50:50 beam splitter, known as Hong-Ou-Mandel (HOM) interference [21], is the most attractive due to its crucial role in some promising applications such as linear-optics quantum computation [5,6] and quantum key distribution [18]. However, due to the lack of high-quality on-demand multiphoton sources [22], it is difficult to implement the HOM interference for more than two photons at a beam splitter, i.e., *generalized* HOM interference [23–26], and to demonstrate high-visibility

quantum interference for a large number of photons. So far, six-photon generalized HOM interference is the largest number of photons reported in previous experiments [12,25–27], and the visibility is only as large as 0.92 [27].

Recently, based on the proposal in Ref. [28], Aragonés *et al.* [29] demonstrated that the outcome of two-photon HOM interference could be bounded with high visibility using phase-randomized weak coherent states (WCSs). The single-photon state tomography can also be probed using phase-randomized WCSs [30]. Combining the decoy-state method [31,32] with the detector-decoy method [33], Navarrete *et al.* [34] proposed a scheme of characterizing MQI in general optical networks (ONs) with high visibility. However, the accuracy of the estimation dramatically decreases for the generalized HOM interference for a large number of photons. The highest number of photons estimated in [34] was limited to 6. The decrease in accuracy is due to the requirement of the optimization of both decoy-state settings and detector-decoy settings. That is, the estimation complexity increases exponentially with the number of photons at each input port.

In this paper, we propose a more efficient method to tightly bound generalized HOM quantum interference. The main goal of the proposed method is to provide a feasible scheme to realize high-visibility quantum interference for a large number of photons, e.g., using phase-randomized WCPs to estimate the statistics provided by ideal n -photon sources. Different from the method used in Ref. [34], we use photon-number-resolving (PNR) detectors to monitor the photon distribution of the output of beam splitters. Thanks to the information provided by the PNR detectors, our method can place a nearly tight analytical bound on the conditional probability

*feihuxu@ustc.edu.cn

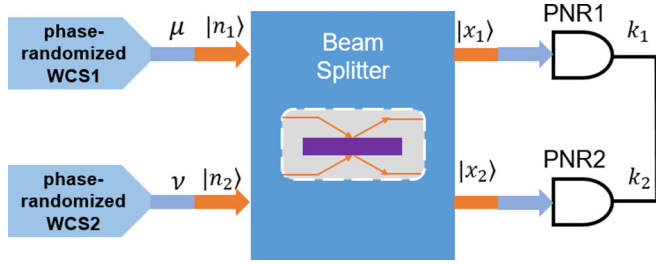


FIG. 1. The schematic diagram of our method for generalized HOM quantum interference. The set of phase-randomized WCSs with different mean photon numbers, μ and ν , is used to estimate the statistics provided by ideal n -photon sources, and n_j (x_j) represents the photon number at the j th input (output) port of the beam splitter. The PNR detectors with single-photon detection efficiency η are placed at the output of the beam splitter to measure the photon number of the output signals. k_1 and k_2 denote the photon numbers observed by the two detectors, respectively.

distribution $P(x_1, x_2|n_1, n_2)$ of the generalized HOM interference. Here, $|n_1, n_2\rangle$ and $|x_1, x_2\rangle$, respectively, denote the input and output of Fock states at the beam splitter. Our numerical simulation shows that our method can demonstrate a large number of photons interference, and is robust against practical errors introduced by imperfections of experiments. Importantly, considering a transition edge sensor (TES) detector that can resolve up to 16 photons [35], we predict that our method can bound 30-photon interference with high visibility and high error tolerances. For the best known TES detector, which has a resolution of 29 photons [36], the proposed method can demonstrate generalized HOM for 56 photons with visibility 99.4%. In practice, our method is useful for several information tasks. For instance, in computation tasks, such as boson sampling [8–12], we can simulate the circuit by inputting WCSs. In measurement device independent quantum key distribution (QKD) [18], since our method can tightly estimate the yield of two single-photon pulses, it can be applied to increase the key rate.

II. METHOD

In this section, we present a general method to tightly bound generalized HOM quantum interference for a large number of photons. Figure 1 shows the schematic diagram of the proposed method. We use phase-randomized WCSs, together with the decoy-state method, as the input, and we employ PNR detectors at the outputs. The fundamental idea of our method is twofold: (i) The decoy-state method can give us precise information on the statistics of the input photon numbers [31,32]; and (ii) the PNR detector has photon-number-resolving capability, thus it can precisely measure the output photon numbers [35,37,38]. Here, we assume that the beam splitter is lossless.

More precisely, we use phase-randomized WCSs with mean photon number μ (ν) at the first (second) input port. Therefore, we can assume the input state $|n_1, n_2\rangle$ is obtained with the probability $p_{n_1}^\mu p_{n_2}^\nu$, where $p_n^\mu = e^{-\mu} \mu^n / n!$ is the photon-number distribution of phase-randomized WCSs given the intensity μ , and the output state can be written as $|x_1, x_2\rangle$ in the Fock state basis, where x_j represents the photon

number at the j th output port. Then the generalized HOM quantum interference can be characterized by the conditional probability distribution $P(x_1, x_2|n_1, n_2)$. Note that here, the lossless assumption of the beam splitter is satisfied by $n_1 + n_2 = x_1 + x_2$. That is, the total number of output photons should be equal to the total number of input photons to the beam splitter.

To estimate the unknown probabilities $P(x_1, x_2|n_1, n_2)$, we can measure the photon number of the output signals by two PNR detectors. However, for a practical PNR detector, such as transition edge sensor (TES) detectors [35,37,38], it has limited quantum efficiency η (typically $\eta < 1$) and finite number resolution of photons. We first consider the semiperfect case where the PNR detectors have the capability to distinguish an infinite number of photons with a detection efficiency $\eta < 1$ [39]. In this situation, the conditional probability of observing k_j photons among x_j photons is $P(k_j|x_j) = C_{x_j}^{k_j} \times \eta^{k_j} (1-\eta)^{x_j-k_j}$. Therefore, for a particular detection outcome (k_1, k_2) , the probability $P_{k_1, k_2}^{\mu, \nu}$ given the input intensities μ, ν is

$$P_{k_1, k_2}^{\mu, \nu} = \sum_{\substack{n_1, n_2 \geq 0 \\ n_1 + n_2 = x_1 + x_2 \\ x_1 \geq k_1, x_2 \geq k_2}} P(k_2|x_2)P(k_1|x_1)P(x_1, x_2|n_1, n_2)p_{n_1}^\mu p_{n_2}^\nu. \quad (1)$$

This is the only information that one can directly obtain from the experiment. It relates the observed probabilities, $P_{k_1, k_2}^{\mu, \nu}$, to the unknown conditional probabilities $P(x_1, x_2|n_1, n_2)$ via the statistics $p_{n_1}^\mu p_{n_2}^\nu$ and $P(k_2|x_2)P(k_1|x_1)$, which are both known *a priori* given the experimental parameters μ, ν, k_1, k_2 , and η . Then by setting up different values of intensity (μ_i, ν_i) , each intensity setting provides a new linear equation that has the same unknowns $P(x_1, x_2|n_1, n_2)$ but different coefficients $p_{n_1}^{\mu_i} p_{n_2}^{\nu_i}$ and $P(k_2|x_2)P(k_1|x_1)$. Solving these sets of linear equations given by $P_{k_1, k_2}^{\mu_i, \nu_i}$, one can estimate any conditional probability $P(x_1, x_2|n_1, n_2)$. However, as we can see from $P_{k_1, k_2}^{\mu_i, \nu_i}$, there is a probability that the input states of the beam splitter are vacuum states, which means that there is no photon interference between the two input modes of the beam splitter. To avoid this situation, one can set up two extra vacuum states $(\mu_i, 0)$ and $(0, \nu_i)$ for each setting (μ_i, ν_i) , and calculate $\bar{B}_{k_1, k_2}^{\mu_i, \nu_i} = e^{-(\mu_i + \nu_i)} P_{k_1, k_2}^{\mu_i, \nu_i} - e^{-\nu_i} P_{k_1, k_2}^{0, \nu_i} - e^{-\mu_i} P_{k_1, k_2}^{\mu_i, 0}$, which is

$$\bar{B}_{k_1, k_2}^{\mu_i, \nu_i} = \sum_{\substack{n_1, n_2 \geq 1 \\ n_1 + n_2 = x_1 + x_2 \\ x_1 \geq k_1, x_2 \geq k_2}} \frac{\mu_i^{n_1} \nu_i^{n_2}}{n_1! n_2!} P(k_2|x_2)P(k_1|x_1)P(x_1, x_2|n_1, n_2). \quad (2)$$

Noticing that, $\bar{B}_{k_1, k_2}^{\mu_i, \nu_i}$ still has many unwanted terms that dramatically decrease the accuracy of the estimation of $P(x_1, x_2|n_1, n_2)$. Here, we take an example of 30-photon interference, $P(15, 15|n_1, n_2)$. In that case, the biggest contribution to $\bar{B}_{15, 15}^{\mu_i, \nu_i}$ are the terms of 31-photon interference. More than 31-photon interference will also contribute to $\bar{B}_{15, 15}^{\mu_i, \nu_i}$, but this contribution is minor because the probability of having more than 31 input photons is much smaller than the probability of having 30 input photons. To obtain a tight estimation of $P(15, 15|n_1, n_2)$ for a small number of intensity settings, we need to cancel out the contribution of

31-photon interference. This can be easily carried out by calculating $\tilde{B}_{15,15}^{\mu_i, \nu_i} - C_1 \tilde{B}_{16,15}^{\mu_i, \nu_i} - C_2 \tilde{B}_{15,16}^{\mu_i, \nu_i}$, where $C_1 = 16(1 - \eta)/\eta$ and $C_2 = 16(1 - \eta)/\eta$, and we denote this calculation as $\tilde{B}_{15,15}^{\mu_i, \nu_i}$. Therefore, $\tilde{B}_{15,15}^{\mu_i, \nu_i}$ only contains the terms of 30-photon interference, and the terms of more than 31-photon interference which make a minor contribution to our final results can be tightly bound to increase the accuracy of the estimation.

Based on the above analysis, the tight estimation of the conditional probability can be solved from the set of linear equations given by $\tilde{B}_{k_1, k_2}^{\mu_i, \nu_i}$. More precisely, from the detection outcome (k_1, k_2) , the conditional probability of K -photon interference, $P(k_1, k_2|j, K - j)$, where $K = k_1 + k_2$ and $1 \leq j \leq K - 1$, could be calculated with $K - 1$ intensity settings (see Appendix A for further details),

$$P_{\text{test}} = \sum_{i=1}^{K-1} [A^{-1}]_{ji} \times \frac{j!(K-j)!}{a_i(\nu_i \eta)^K} \times \tilde{B}_{k_1, k_2}^{a_i \nu_i, \nu_i}. \quad (3)$$

Here, we have $a_i = \mu_i/\nu_i$ and $U_i = \mu_i + \nu_i$ for the i th decoy-state setting. The term $[A^{-1}]_{ji}$ is an element of the inverse of the Vandermonde matrix [see Eq. (A5)] and $\tilde{B}_{k_1, k_2}^{a_i \nu_i, \nu_i} = \tilde{B}_{k_1, k_2}^{a_i \nu_i, \nu_i} - C_1 \tilde{B}_{k_1+1, k_2}^{a_i \nu_i, \nu_i} - C_2 \tilde{B}_{k_1, k_2+1}^{a_i \nu_i, \nu_i}$, where $C_1 = (k_1 + 1)(1 - \eta)/\eta$ and $C_2 = (k_2 + 1)(1 - \eta)/\eta$. The lower and upper bounds of the estimation are set by

$$\Delta_{\pm} = \frac{\Delta_2 \pm \Delta_1}{2}. \quad (4)$$

The terms Δ_1 and Δ_2 , which are given in Appendix B, denote the contributions of more than $(K + 1)$ -photon interference. Hence, the conditional probability, $P(k_1, k_2|j, K - j)$, can be expressed by

$$P_{\text{test}} + \Delta_- < P(k_1, k_2|j, K - j) < P_{\text{test}} + \Delta_+. \quad (5)$$

To get the best estimation, one needs to optimize $\{a_i\}$ and $\{U_i\}$. Since there exist $2(K - 1)$ parameters to be optimized, the performance of the numerical optimization is very low. Here, we provide a special optimization method. In our model, when phase-randomized WCSs are used to simulate Poisson distributions of Fock states, the probability of getting the state $|n_1, n_2\rangle$ is $p_{n_1}^{\mu} p_{n_2}^{\nu}$. After letting $\mu = a\nu$, $U = \mu + \nu$, and $a = n_1/n_2$, this probability then reaches its maximum value. Therefore, in the calculation of the conditional probabilities $P(k_1, k_2|n, K - n)$, $a_n = n/(K - n)$. For $n = (1, \dots, K - 1)$, there exists $K - 1$ different values of a_n . For each a_n , we could let U_n be a constant U which is less than 1, which is a valid setting that could still provide high accuracy.

The proposed method can also be used to characterize any ONs with N input ports and L output ports. However, the estimation complexity may increase exponentially with the number of input/output ports of the ON (see Appendixes A and C for further details).

III. SIMULATION

To illustrate the practicality of our method, We first calculate two simple examples $P(15, 15|2, 28)$ and $P(28, 28|2, 54)$. Then we use an example of 100-photon interference to show that our method could evaluate a large number of photon interference if the working-accuracy of the computer is high enough. To run the simulations, we take a toy model from

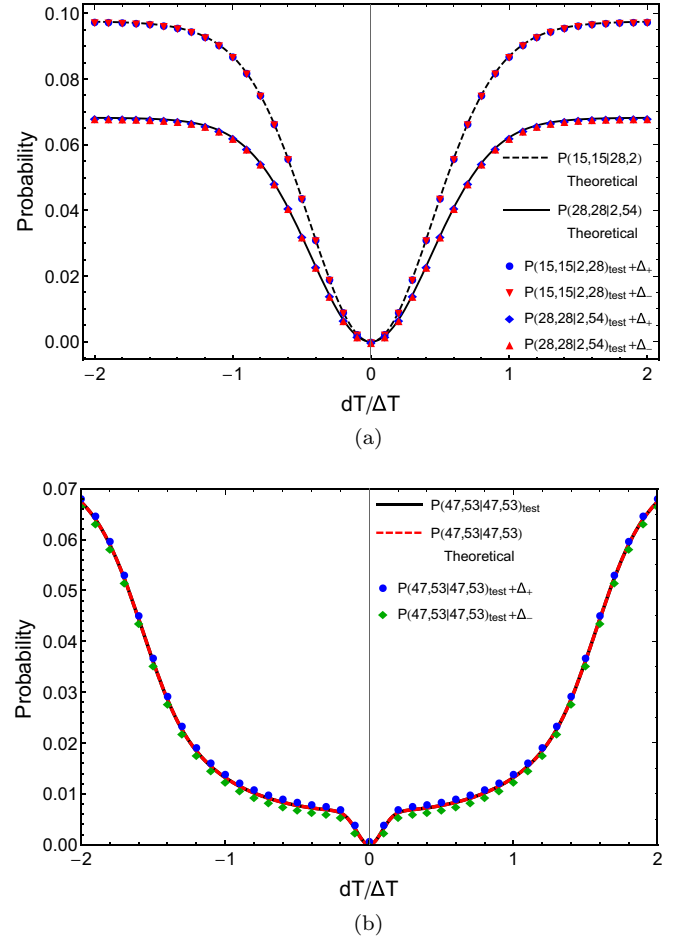


FIG. 2. Generalized Hong-Ou-Mandel dip for different conditional probabilities. $dT/\Delta T$ is the the relative delay. In these simulations, $\eta = 0.9$ and $U = 0.1$. (a) $P(28, 28|2, 54)_{\text{test}}$ and $P(15, 15|2, 28)_{\text{test}}$ at a beam splitter of transmittance $t = 0.432580$ and 0.407152 , respectively. For $P(15, 15|2, 28)$, the upper and lower bound of the estimation, $\Delta_{\pm} = (2.96 \times 10^{-5}, -3.86 \times 10^{-6})$ and for $P(28, 28|2, 54)$, $\Delta_{\pm} = (2.74 \times 10^{-5}, -1.93 \times 10^{-6})$. (b) $P(47, 53|47, 53)_{\text{test}}$ at a beam splitter of transmittance $t = 0.606364$.

Ref. [34], where the spectrum of phase-randomized weak coherent pulses follows a Gaussian distribution. For the theoretical values in our simulation, they are calculated by the corresponding P_{test} with $\eta = 1$ (see Appendix D for details).

Figure 2(a) shows simulated probabilities $P(15, 15|2, 28)$ and $P(28, 28|2, 54)$ at a beam splitter as a function of the relative delay $dT/\Delta T$, respectively, where we have made an assumption that two PNR detectors can distinguish infinite photons. Here, dT is the absolute delay between the arrival times of the input pulses at each input port of the beam splitter, while ΔT is the full width at half-maximum (FWHM) of the pulses, which we assume is the same for all inputs for simplicity. For these two cases, we let the transmittance of the beam splitter be $t = 0.407152$ and 0.432580 , respectively. Then, when the relative delay is zero, quantum mechanics predicts that both these two conditional probabilities are zero. We can see that the simulated results fit the theoretical values very well.

For characterizing generalized HOM quantum interference for a large number of photons, because the probability of having large input photons from the coherent states drop quickly to zero, we need to perform simulations involving decimals at a high level of accuracy, i.e., high-accuracy computation. That is, consider a coherent state with a mean photon number of 1, the probability to measure 54 photons in this state is of the order 10^{-72} . To run the simulations, it is necessary to ensure that the experimental parameters should have the same accuracy, i.e., 10^{-72} , which can be implemented by adding 0 after the decimal part of the parameters. Figure 2(b) shows the estimation of 100-photon interference, $P(47, 53|47, 53)$, as an example, where the theoretical value is illustrated with black line. Because the upper and lower bounds illustrated in Fig. 2(b), Δ_{\pm} are both $O(10^{-4})$, the calculated conditional probabilities are extremely close to the theoretical results. This numerical simulation suggest that with high-accuracy computation, our method can efficiently characterize a large number of photons interference.

These three numerical simulations suggest that with high-accuracy computation, our method can efficiently characterize infinite-photon interference. Also, we emphasize that the upper and lower bounds illustrated in Fig. 2 do not depend on the absolute value of $dT/\Delta T$ (see Appendix B for further details).

IV. PRACTICAL ERRORS

In experiment, the beam splitter transitivity t , single-photon detection efficiency η , and total mean photon number U may have errors that are different from the assumed value, i.e., η may be 0.88 instead of 0.90 as assumed in theory. This is because it is impossible to perfectly characterize a parameter in experiment. Since the analytical expression of the conditional probability is a function of (η, t, U) , it is necessary to estimate the influence of the variation on these parameters.

By defining the deviation $(\Delta\eta, \Delta t, \Delta U)$, one can have the contour map of

$$P_{\text{test}}(\eta_0, t_0, U_0) - P_{\text{test}}(\eta_0 + \Delta\eta, t_0 + \Delta t, U_0 + \Delta U). \quad (6)$$

This value can be seen as a source of the practical errors. Here, (η_0, t_0, U_0) is the working point and $(\Delta\eta, \Delta t, \Delta U)$ defined by $(\eta - \eta_0, t - t_0, U - U_0)$ is the absolute error.

Figure 3 shows the practical errors of $P(15, 15|2, 28)_{\text{test}}$, $P(28, 28|2, 54)_{\text{test}}$, and $P(47, 53|47, 53)_{\text{test}}$. It is easy to find that when $|\Delta t| = 0.1$, the practical error is about $O(10^{-2})$, which is much larger than the errors caused by ΔU and $\Delta\eta$. Thus the practical error mainly depends on the beam ratio t , while U and η do not appear to be a major problem. This is because, in quantum optics, a small deviation of t will significantly influence the interference. Especially, for a large number of photons interference, there are many choices of t to make the conditional probability be 0. For example, when we calculate the situation $P(47, 53|47, 53) = 0$, t could be set to 0.545 185, 0.606 364, 0.636 947, and so on. Since these values are so close to each other, the practical error about t is concussive [see Fig. 3(c)]. Furthermore, we also investigate how the choice of U and η affects Δ_{\pm} . See Appendix E for details.

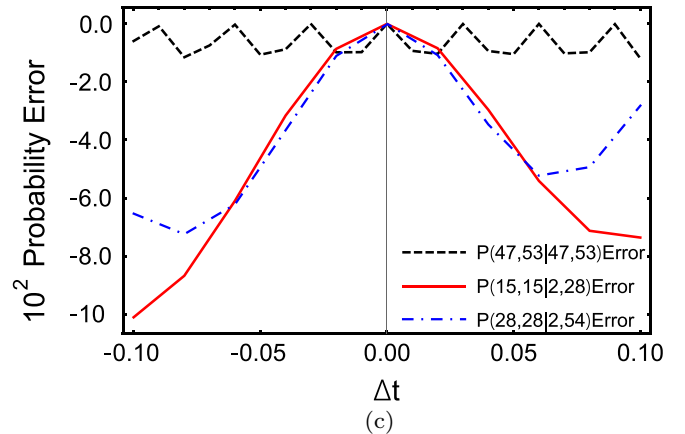
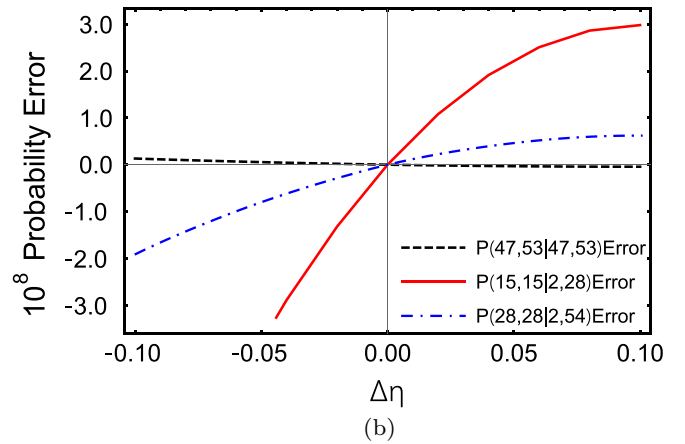
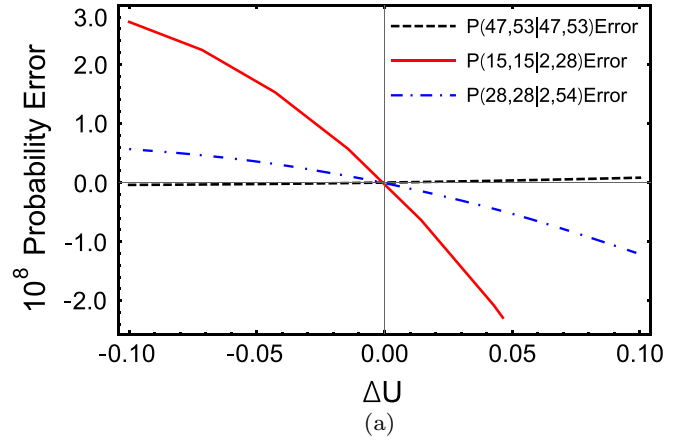


FIG. 3. Practical errors for the conditional probabilities. The solid red, dashed black, and dot-dashed blue lines represent the simulation of $P(15, 15|2, 28)_{\text{test}}$, $P(47, 53|47, 53)_{\text{test}}$, and $P(28, 28|2, 54)_{\text{test}}$, respectively, whose working points are $(0.9, 0.407152, 0.1)$, $(0.9, 0.606364, 0.1)$, and $(0.9, 0.432580, 0.1)$, respectively. Parts (a), (b), and (c) are practical errors about U , η , and t , respectively.

V. METHOD FOR PRACTICAL DETECTORS

In experiment, the practical PNR detectors, such as TES detectors, can only resolve a finite number of photons. To our knowledge, the resolved number of photons is up to 29 [36]. In this section, we focus on how to tightly bound the

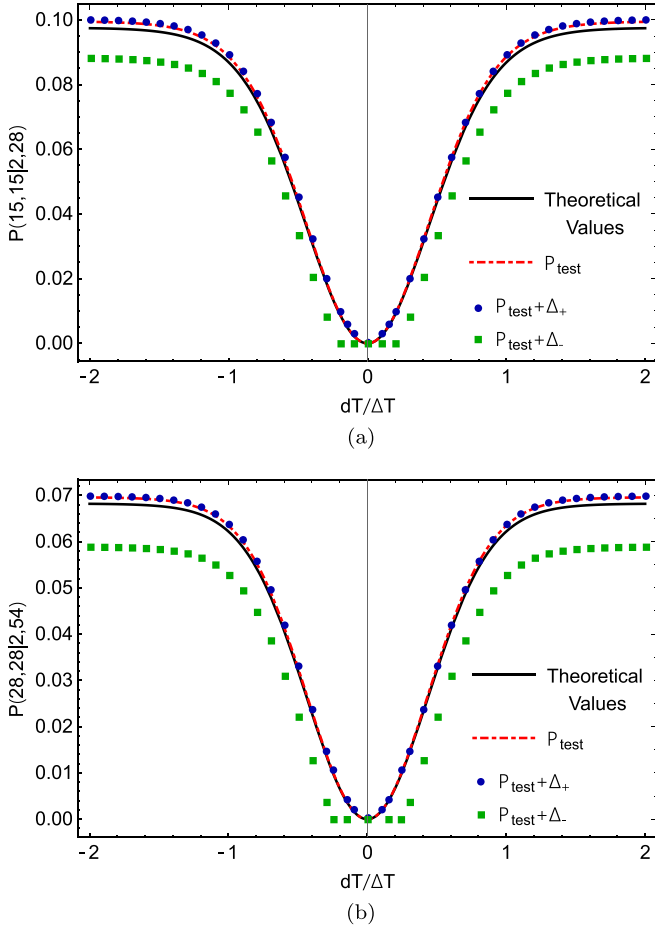


FIG. 4. (a) Generalized HOM dip for $P(15, 15|2, 28)$ () with two practical TES detectors that cannot distinguish more than 16 photons, where $\Delta_{\pm} = (0.000\ 754, -0.011\ 156)$, $t = 0.407\ 152$, $U = 0.1$, and $\eta = 0.8$. (b) HOM dip for $P(28, 28|2, 54)$ with two practical TES detectors that cannot distinguish more than 29 photons, where $\Delta_{\pm} = (0.000\ 384, -0.010\ 655)$, $t = 0.432\ 580$, $U = 0.1$, and $\eta = 0.8$.

generalized HOM quantum interference when the detector has finite resolution of the number of photons.

As mentioned in Sec. II, the information provided by the TES detector is used to bound the conditional probabilities. If the detectors can only resolve up to S photons, the detector could not distinguish more than S photons. In this situation, the conditional probability of observing S photons among $x_j (> S)$ photons should be modified as $P(S|x_j) = \sum_{y=S}^{x_j} C_{x_j}^y \times \eta^y (1 - \eta)^{x_j - y}$. Then the terms such as $B_{S,k}^{\mu\nu}$ and $B_{k,S}^{\mu\nu}$ will be changed into the form of $\sum_{l=S}^{\infty} \bar{B}_{l,k}^{\mu\nu}$ and $\sum_{l=S}^{\infty} \bar{B}_{k,l}^{\mu\nu}$, respectively, where $k < S$. If we use these two terms to reduce the contribution of unwanted terms, the accuracy of the estimation will decrease (see Appendix B). Therefore, the terms $\bar{B}_{S,k}^{\mu\nu}$ and $(\bar{B}_{k,S}^{\mu\nu})$ could be ignored and $P(S - 1, k|j, K - j)_{\text{test}}$ can be modified as

$$\sum_{i=1}^{K-1} [A^{-1}]_{ji} \frac{j!(K-j)!}{a_i(v_i\eta)^K} \times (\bar{B}_{S-1,k}^{a_i v_i, v_i} - C_2 \bar{B}_{S-1,k+1}^{a_i v_i, v_i}), \quad (7)$$

where S, k, K satisfies the condition $S - 1 + k = K$, and $j = 1, \dots, K - 1$. The difference between Eq. (7) and Eq. (3)

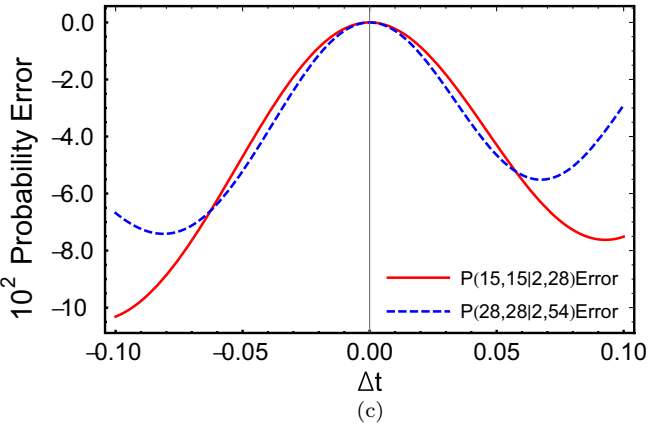
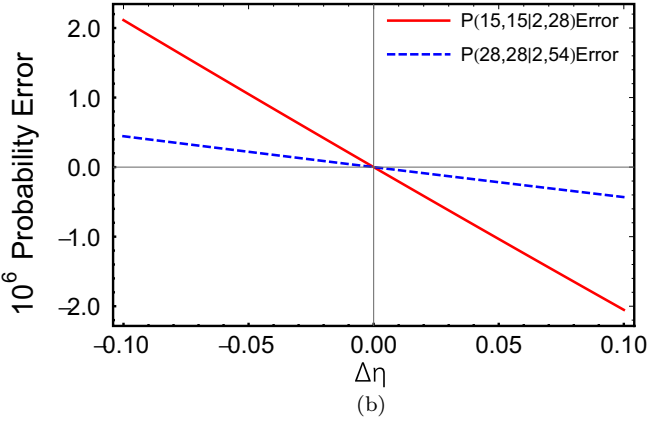
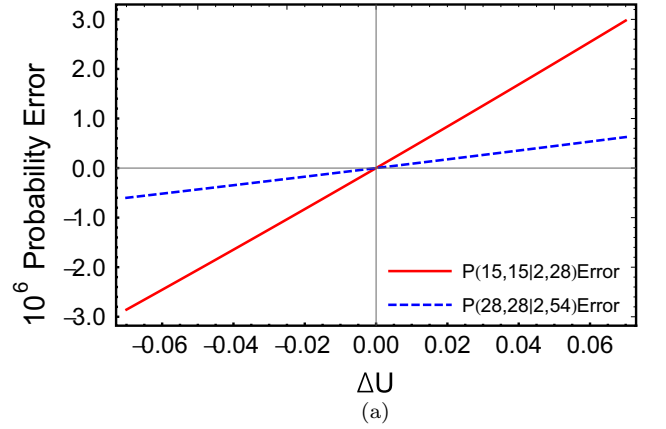


FIG. 5. Practical errors for the conditional probability. The solid red and dashed blue lines represent the simulation of $P(15, 15|2, 28)_{\text{test}}$ and $P(28, 28|2, 54)_{\text{test}}$, respectively. Parts (a), (b), and (c) are practical errors about U, η , and t , respectively. For $P(15, 15|2, 28)_{\text{test}}$ and $P(28, 28|2, 54)_{\text{test}}$, the working points are $(0.8, 0.407\ 152, 0.1)$ and $(0.8, 0.432\ 580, 0.1)$.

is that we just let $C_1 = 0$. So, for different detection results (k_1, k_2) , one can modify C_1 and C_2 as

$$C_1 = \begin{cases} (k_1 + 1)^{\frac{1-\eta}{\eta}}, & k_1 \leq S - 2, \\ 0, & k_1 \geq S - 1, \end{cases} \quad C_2 = \begin{cases} (k_2 + 1)^{\frac{1-\eta}{\eta}}, & k_2 \leq S - 2, \\ 0, & k_2 \geq S - 1. \end{cases} \quad (8)$$

After this modification, one could take the same approach for $P(k, S-1|j, K-j)$ and $P(S-1, S-1|j, K-j)$. Using this approach, any probability $P(k_1, k_2|n_1, n_2)$ that satisfies $k_1 \leq S-1$ and $k_2 \leq S-1$ could be easily calculated.

In our simulation, we consider two cases in which the TES can resolve different numbers of photons. In the first case, we consider a TES that resolves up to 16 photons [35]. Our method predicts that one can evaluate a maximum 30-photon interference, the conditional probabilities of which are in the form $P(15, 15|n, 30-n)$, where $n = 1, \dots, 15$. In the second case, we consider the best reported TES in Ref. [36], which can resolve up to 29 photons. Figures 4(a) and 4(b) show the HOM dip of $P(15, 15|2, 28)$ and $P(28, 28|2, 54)$. The difference between the predictions of quantum and classical mechanics can be quantified by means of the visibility [34], which could be as large as $0.992_{-0}^{+0.008}$. Because these two TES detectors cannot provide information on 31 photons, we cannot decrease their contribution. The contribution of more than 30-photon interference leads to a huge deviation between the lower bound (green squares) and its theoretical value (solid black line) compared to Fig. 2(a). However, according to Fig. 5, the practical errors are still primarily dependent on the beam ratio t , while U and η have little influence on it. The 56-photon interference, as shown in Fig. 4(b), has the same performance as 30-photon interference, and the visibility is around $0.994_{-0}^{+0.006}$.

VI. CONCLUSION

In summary, we propose an experimentally implementable proposal for demonstrating the generalized HOM interference for a large number of photons with high visibility. In our proposal, we use phase-randomized weak coherent states and practical PNR detectors, both of which can be implemented with current technology. Furthermore, our method could be used to obtain a tight bound in the input-output photon number statistics of a beam splitter, and no numerical optimization is required.

To illustrate the practicality of the method, we examine three examples: 30-photon interference, 56-photon interference, and 100-photon interference. In these three cases, we obtain high-accuracy estimations of theoretical values. Considering the flaws in the actual experiment, we analyze the practical errors and find that they are mainly dependent on the beam splitter transmissivity t , while the total mean photon number U and detector efficiency η have little influence on it. To further extend our method, we also provide a modified model for the detector with finite-number resolution of photons. For detectors that cannot distinguish more than S photons, it is possible to demonstrate $2(S-1)$ -photon interference at most.

ACKNOWLEDGMENTS

We thank Yang Liu, Chenglong You, and Jia-Qiang Zhong for helpful discussions. This work was supported by National Key R&D Program of China (SQ2018YFB050100), the National Natural Science Foundation of China (Grants No. 61771443 and No. 61705048), the Thousand Young Talent Program of China, Fundamental Research

Funds for the Central Universities (WK2340000083), Shanghai Science and Technology Development Funds (18JC1414700), and the Guangxi Science Foundation (Grant No. 2017GXNSFBA198231).

APPENDIX A: CALCULATION OF P_{test}

Before we calculate P_{test} , we denote as $K = k_1 + k_2$ the total number of photons observed by the two PNR detectors. To cancel out the contribution of $(K+1)$ -photon interference and reduce the contribution of more than $(K+2)$ -photon interference, we calculate a new term $\tilde{B}_{k_1 k_2}^{\mu\nu}$, which is given by

$$\begin{aligned} \tilde{B}_{k_1, k_2}^{\mu\nu} &= \bar{B}_{k_1, k_2}^{\mu\nu} - C_1 \bar{B}_{k_1+1, k_2}^{\mu\nu} - C_2 \bar{B}_{k_1, k_2+1}^{\mu\nu} \\ &= \sum_{n_1=1}^{K-1} \frac{\mu^{n_1} \nu^{K-n_1}}{n_1!(K-n_1)!} \eta^K P(k_1, k_2|n_1, K-n_1) - \Delta_{k_1 k_2}^{\mu\nu}, \end{aligned} \quad (\text{A1})$$

where the coefficients C_1 and C_2 satisfy

$$\begin{aligned} C_1 &= (k_1 + 1) \times \frac{1 - \eta}{\eta}, \\ C_2 &= (k_2 + 1) \times \frac{1 - \eta}{\eta}, \end{aligned} \quad (\text{A2})$$

and

$$\begin{aligned} \Delta_{k_1 k_2}^{\mu\nu} &= - \sum_{M \geq K+2} \sum_{n_1=1}^{M-1} \frac{\mu^{n_1} \nu^{M-n_1}}{n_1!(M-n_1)!} \\ &\quad \times (Y_{n_1|M-n_1}^{k_1 k_2} - c_1 Y_{n_1|M-n_1}^{k_1+1 k_2} - c_2 Y_{n_1|M-n_1}^{k_1 k_2+1}), \end{aligned} \quad (\text{A3})$$

and $Y_{n_1|M-n_1}^{k_1 k_2}$ is equal to

$$\begin{aligned} Y_{n_1|M-n_1}^{k_1 k_2} &= \sum_{\substack{x_1+x_2=M \\ x_1 \geq k_1 \\ x_2 \geq k_2}} C_{x_1}^{k_1} C_{x_2}^{k_2} \eta^{k_1} (1-\eta)^{x_1-k_1} \\ &\quad \times \eta^{k_2} (1-\eta)^{x_2-k_2} P(x_1, x_2|n_1, n_2) \\ &= \sum_{x_1=k_1}^{M-k_2} C_{x_1}^{k_1} C_{M-x_1}^{k_2} \times \eta^K (1-\eta)^{M-K} \\ &\quad \times P(x_1, M-x_1|n_1, M-n_1). \end{aligned}$$

Each intensity setting provides a new linear equation that has the same unknowns $P(k_1, k_2|n_1, K-n_1)$ but with different coefficients. By setting up $K-1$ different values of intensity (μ_i, ν_i) and solving the set of linear equations, one can estimate any conditional probability $P(k_1, k_2|n_1, K-n_1)$. The result can be expressed as

$$\begin{aligned} P(k_1, k_2|j, K-j) &= \sum_{i=1}^{K-1} [A^{-1}]_{ji} \frac{j!(K-j)!}{a_i(\nu_i \eta)^K} \tilde{B}_{k_1, k_2}^{a_i \nu_i, \nu_i} \\ &\quad + \sum_{i=1}^{K-1} [A^{-1}]_{ji} \frac{j!(K-j)!}{a_i(\nu_i \eta)^K} \Delta_{k_1 k_2}^{a_i \nu_i, \nu_i}, \end{aligned} \quad (\text{A4})$$

where $[A^{-1}]_{ji}$ is

$$[A^{-1}]_{ji} = (-1)^{j+1} \frac{\sum_{1 \leq p_1 \leq p_2 \leq \dots \leq p_{K-1-j} \neq i} a_{p_1} a_{p_2} \dots a_{K-1-j}}{\prod_{1 \leq l \leq K-1} (a_l - a_i)}, \quad (\text{A5})$$

which is an element of the inverse of the Vandermonde matrix. In our simulations, we use the symmetric functions [40] to calculate Eq. (A5). Here, we have set $\mu_i = a_i v_i$ ($a_i > 0$) and $U_i = \mu_i + v_i$, where U_i is the mean of the total photon number of the input state. Because $\tilde{B}_{k_1 k_2}^{\mu\nu}$ could be obtained directly from the experiment, $P(k_1, k_2|j, K-j)$ can be estimated by the first term of Eq. (A4),

$$P_{\text{test}} = \sum_{i=1}^{K-1} [A^{-1}]_{ji} \times \frac{j!(K-j)!}{a_i(v_i\eta)^K} \times \tilde{B}_{k_1 k_2}^{a_i v_i, v_i}. \quad (\text{A6})$$

The lower and upper bounds of $P(k_1, k_2|j, K-j)$ denoted by (Δ_-, Δ_+) can be deduced from the second term of Eq. (A4), which can be denoted by

$$\Delta = \sum_{i=1}^{K-1} [A^{-1}]_{ji} \times \frac{j!(K-j)!}{a_i(v_i\eta)^K} \times \Delta_{k_1 k_2}^{a_i v_i, v_i}. \quad (\text{A7})$$

We will show more details on how to estimate this bound with strict mathematical proof in Appendix B.

APPENDIX B: UPPER AND LOWER BOUNDS

Before we derive the upper and lower bounds, we first prove $\Delta_{k_1 k_2}^{\mu\nu} \geq 0$. From Appendix A, for 2-2 ONs, $\Delta_{k_1 k_2}^{\mu\nu}$ has the form

$$\Delta_{k_1 k_2}^{\mu\nu} = - \sum_{M \geq K+2} \sum_{n_1=1}^{M-1} \frac{\mu^{n_1} v^{M-n_1}}{n_1!(M-n_1)!} \times (Y_{n_1|M-n_1}^{k_1 k_2} - c_1 Y_{n_1|M-n_1}^{k_1+1 k_2} - c_2 Y_{n_1|M-n_1}^{k_1 k_2+1}).$$

If we define $\varepsilon_1, \varepsilon_2$, and ε_3 as

$$\varepsilon_1 = \{(k_2 + 1)C_{M-k_1}^{k_2+1} - C_{M-k_1}^{k_2}\} \times P(k_1, M - k_1|n_1, M - n_1),$$

$$\varepsilon_2 = \{(k_1 + 1)C_{M-k_2}^{k_1+1} - C_{M-k_2}^{k_1}\} \times P(M - k_2, k_2|n_1, M - n_1),$$

$$\varepsilon_3 = \sum_{x_1=k_1+1}^{M-k_2-1} \{(k_1 + 1)C_{x_1}^{k_1+1} C_{M-x_1}^{k_2} + (k_2 + 1)C_{x_1}^{k_1}\} \times \{C_{M-x_1}^{k_2+1} - C_{x_1}^{k_1} C_{M-x_1}^{k_2}\} P(x_1, M - x_1|n_1, M - n_1),$$

by using these terms, $\Delta_{k_1 k_2}^{\mu\nu}$ can be written as

$$\Delta_{k_1 k_2}^{\mu\nu} = \sum_{M \geq K+2} \sum_{n_1=1}^{M-1} \frac{\mu^{n_1} \times v^{M-n_1}}{n_1!(M-n_1)!} \eta^K (1-\eta)^{M-K} \times (\varepsilon_1 + \varepsilon_2 + \varepsilon_3). \quad (\text{B1})$$

It is easy to find out that, when using the function $(k+1)C_x^{k+1} = (x-k)C_x^k$ to simplify $\varepsilon_1, \varepsilon_2$, and ε_3 , we will have

$$\varepsilon_1 = (M - K - 1)C_{M-k_1}^{k_2} P(k_1, M - k_1|n_1, M - n_1),$$

$$\varepsilon_2 = (M - K - 1)C_{M-k_2}^{k_1} P(M - k_2, k_2|n_1, M - n_1),$$

$$\varepsilon_3 = \sum_{x_1=k_1+1}^{M-k_2-1} (M - K - 1)C_{x_1}^{k_1} C_{M-x_1}^{k_2} \times P(x_1, M - x_1|n_1, M - n_1).$$

Therefore, for any $M \geq K + 2$, the term $\varepsilon_1 + \varepsilon_2 + \varepsilon_3 \geq 0$, then $\Delta_{k_1 k_2}^{\mu\nu} \geq 0$, and the maximum value of the term $\varepsilon_1 + \varepsilon_2 + \varepsilon_3, \varepsilon_M, \text{ is}$

$$\varepsilon_M := \max_{1 \leq n_1 \leq M-1} (\varepsilon_1 + \varepsilon_2 + \varepsilon_3) = (M - K - 1)C_{x_1}^{k_1} C_{M-x_1}^{k_2} |_{x_1 = \lfloor \frac{k_1}{k_1+k_2} \times M \rfloor}, \quad (\text{B2})$$

with $P(x_1, M - x_1|n_1, M - n_1)$ satisfying

$$P(x_1, M - x_1|n_1, M - n_1) = \begin{cases} 1, & x_1 = \lfloor \frac{k_1}{k_1+k_2} \times M \rfloor, \\ 0, & x_1 \neq \lfloor \frac{k_1}{k_1+k_2} \times M \rfloor, \end{cases} \quad (\text{B3})$$

which is not determined by the structure ONs.

To obtain the lower bound Δ_- and upper bound Δ_+ of Δ , we define Δ_1 and Δ_2 from Eqs. (A7), (B1), and (B2), that is,

$$\Delta_1 = \sum_{M \geq K+1} \sum_{n_1=1}^{M-1} \frac{j!(K-j)!}{n_1!(M-n_1)!} [(1-\eta)U]^{M-K} \times \left| \sum_{i=1}^{K-1} [A^{-1}]_{ji} \frac{a_i^{n-1}}{(a_i+1)^{M-K}} \right| \times \varepsilon_M,$$

$$\Delta_2 = \sum_{M \geq K+1} \sum_{n_1=1}^{M-1} \frac{j!(K-j)!}{n_1!(M-n_1)!} [(1-\eta)U]^{M-K} \times \left(\sum_{i=1}^{K-1} [A^{-1}]_{ji} \frac{a_i^{n-1}}{(a_i+1)^{M-K}} \right) \times \varepsilon_M. \quad (\text{B4})$$

Therefore, $(\Delta_2 \pm \Delta_1)/2$ are related to the positive part and negative part of Δ , respectively. Thus Δ will satisfy

$$(\Delta_2 - \Delta_1)/2 \leq \Delta \leq (\Delta_1 + \Delta_2)/2, \quad (\text{B5})$$

and the upper and lower bounds will be $\Delta_{\pm} = (\Delta_2 \pm \Delta_1)/2$.

It should be noted that, since the restrictive condition (B3) has been used, Δ_+ and Δ_- are mainly dependent on the method of detection model rather than the structure of the ON. We also emphasize that it is sufficient to use just the two terms $\tilde{B}_{k_1+1 k_2}^{\mu\nu}$ and $\tilde{B}_{k_1 k_2+1}^{\mu\nu}$ with coefficients C_1 and C_2 to cancel out the unwanted terms. If we take more terms into the estimation, it is easy to find that the maximum value of $\varepsilon_1 + \varepsilon_2 + \varepsilon_3$ will be increased, which will lead to a decrease in accuracy. Therefore, in the method for the practical TES detectors, we just ignore $\tilde{B}_{S,k}^{\mu\nu}$ and $\tilde{B}_{k,S}^{\mu\nu}$.

APPENDIX C: THE GENERAL INPUT-OUTPUT MODEL FOR N - L OPTICAL NETWORKS

As mentioned in Sec. II, our method can be extended to characterize any optical networks (ON) with N inputs and L outputs. The difficulty behind this extension is that one should find a suitable set of decoy states to solve the linear equations. Here, we just provide the general input-output model for N - L optical networks. This model could be strictly derived by using the positive-operator-valued measure (POVM). We start with the N input state of the ON, which is given by

$$\rho_{\text{in}}^{\mu} = \bigotimes_{i=1}^N \rho_i^{\mu_i} = \sum_{\mathbf{n}} P_{\mathbf{n}}^{\mu} |\mathbf{n}\rangle \langle \mathbf{n}|. \quad (\text{C1})$$

Then the output state of the ON is $\rho_{\text{out}}^{\mu} = \hat{U} \rho_{\text{in}}^{\mu} \hat{U}^{\dagger}$, where \hat{U} denotes the evolution unitary operator given by the ON. Because the practical PNR detector can be modeled as a perfect PNR detector in combination with a *virtual beam splitter* whose transmittance is η , we can define the POVM elements $\hat{\Pi}_{x_j}^{k_j}$ as

$$\hat{\Pi}_{x_j}^{k_j} = \sum_{x_j \geq k_j} P(k_j | x_j) |x_j\rangle \langle x_j|_O \otimes |k_j\rangle \langle k_j|_D \quad (\text{C2})$$

at each port of the detectors. Here, $|x_j\rangle_O$ is the output state of the ON and $|k_j\rangle_D$ can be seen as the output state of the *virtual beam splitter*. $P(k_j | x_j)$ is the probability that characterizes the behavior of the PNR detector. The operator $\hat{\Pi}_{x_j}^{k_j}$ is associated with an observation of k_j photons among x_j photons at the j th detector. Then the general input-output model is given by

$$\begin{aligned} P_{\mathbf{k}}^{\mu} &= \text{Tr}[\hat{\Pi}_{\mathbf{x}}^{\mathbf{k}} \rho_{\text{in}}^{\mu}] \\ &= \sum_{\mathbf{n}} \sum_{\mathbf{x} \geq \mathbf{k}} P_{\mathbf{n}}^{\mu} P(\mathbf{k} | \mathbf{x})_O \langle \mathbf{x} | U | \mathbf{n} \rangle_I \langle \mathbf{n} | U^{\dagger} | \mathbf{x} \rangle_O \\ &= \sum_{\mathbf{n}} \sum_{\mathbf{x} \geq \mathbf{k}} P(\mathbf{k} | \mathbf{x}) P(\mathbf{x} | \mathbf{n}) P_{\mathbf{n}}^{\mu}, \end{aligned} \quad (\text{C3})$$

where $P(\mathbf{x} | \mathbf{n}) = |\langle \mathbf{n} | U^{\dagger} U | \mathbf{x} \rangle_O|^2$ is the conditional probabilities characterizing the behavior of ON. $P_{\mathbf{k}}^{\mu}$ is the probability of observing $\mathbf{k} = (k_1, \dots, k_K)$ photons at the port of the ON given the input intensity $\boldsymbol{\mu} = (\mu_1, \dots, \mu_N)$.

APPENDIX D: TOY MODEL FOR SIMULATIONS

Our toy model comes from Ref. [34], but we replace the single photon detectors by PNR detectors with detection efficiency η . In the case of WCPs, the input state to the beam splitter can be written as $|\psi_{\text{in}}\rangle = |\psi_{\mu,1}\rangle \otimes |\psi_{\nu,2}\rangle$, where

$$\begin{aligned} |\psi_{\mu,1}\rangle &= \exp\left(\int [\mu(\omega)\hat{a}_1^{\dagger}(\omega) - \mu^*(\omega)\hat{a}_1(\omega)]d\omega\right)|0\rangle, \\ |\psi_{\nu,2}\rangle &= \exp\left(\int [\nu(\omega)\hat{a}_2^{\dagger}(\omega) - \nu^*(\omega)\hat{a}_2(\omega)]d\omega\right)|0\rangle \end{aligned} \quad (\text{D1})$$

are the coherent state at the first and second input ports. Here, the parameters $\mu(\omega)$ and $\nu(\omega)$ are defined as

$$\begin{aligned} \mu(\omega) &= \frac{\sqrt{\mu}}{(2\pi\sigma^2)^{1/4}} \exp\left(-\frac{\omega^2}{4\sigma^2}\right) e^{i\phi_1 - \omega t_1}, \\ \nu(\omega) &= \frac{\sqrt{\nu}}{(2\pi\sigma^2)^{1/4}} \exp\left(-\frac{\omega^2}{4\sigma^2}\right) e^{i\phi_2 - \omega t_2}, \end{aligned} \quad (\text{D2})$$

where we have assumed that $|\mu(\omega)|^2$ and $|\nu(\omega)|^2$ follow a Gaussian distribution of mean zero and standard deviation σ which are multiplied by the intensities μ and ν to guarantee the conditions $\int |\mu(\omega)|^2 d\omega = \mu$ and $\int |\nu(\omega)|^2 d\omega = \nu$. The temporal parameters t_1 and t_2 represent the arrival time of the optical pulse that enters the beam splitter.

After the interference, the output states to the beam splitter can be written as $|\psi_{\text{out}}\rangle = |\psi_{\mu',1}\rangle \otimes |\psi_{\nu',2}\rangle$, where

$$\begin{aligned} |\psi_{\mu'}\rangle &= \exp\left(\int [\mu'(\omega)\hat{a}_1^{\dagger}(\omega) - \mu'^*(\omega)\hat{a}_1(\omega)]d\omega\right)|0\rangle, \\ |\psi_{\nu'}\rangle &= \exp\left(\int [\nu'(\omega)\hat{a}_2^{\dagger}(\omega) - \nu'^*(\omega)\hat{a}_2(\omega)]d\omega\right)|0\rangle, \end{aligned} \quad (\text{D3})$$

and the mean photon numbers at the output ports are given by $n_1 = \int |\mu'(\omega)|^2 d\omega$ and $n_2 = \int |\nu'(\omega)|^2 d\omega$. It is then straightforward to show that

$$\begin{aligned} n_1 &= t\mu + (1-t)\nu - 2e^{-\ln(2)\tau^2} \cos(\phi_1 - \phi_2), \\ n_2 &= (1-t)\mu + t\nu + 2e^{-\ln(2)\tau^2} \cos(\phi_1 - \phi_2), \end{aligned} \quad (\text{D4})$$

where $\tau = (t_1 - t_2)/\Delta T$ represents the relative delay between the arrival times of the pulses that enter the beam splitter, and ΔT is the FWHM. When observing k_1 and k_2 photons at each output port, the POVMs of the PNR detectors at the output ports are given by $\hat{\Pi}_1$ and $\hat{\Pi}_2$, where $\hat{\Pi}_i$ is

$$\hat{\Pi}_i = \sum_{x \geq k} C_x^k \eta^k (1-\eta)^k |x\rangle \langle x|_i. \quad (\text{D5})$$

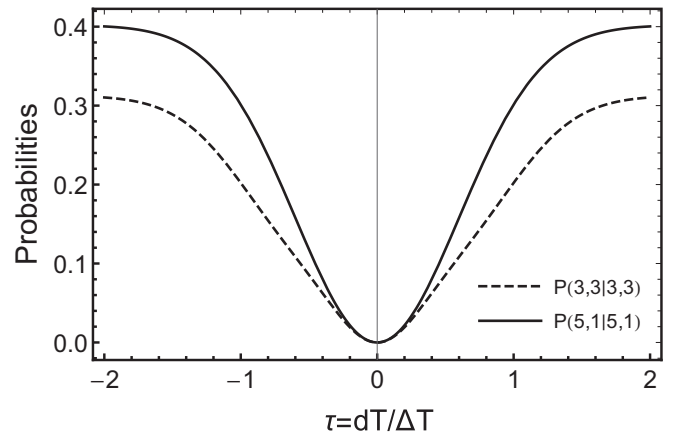


FIG. 6. Theoretical value of Hong-Ou-Mandel dip for the conditional probabilities $P(3, 3|3, 3)$ and $P(5, 1|5, 1)$ at a beam splitter of transmittance $t = 1/2$ and $5/6$, respectively.

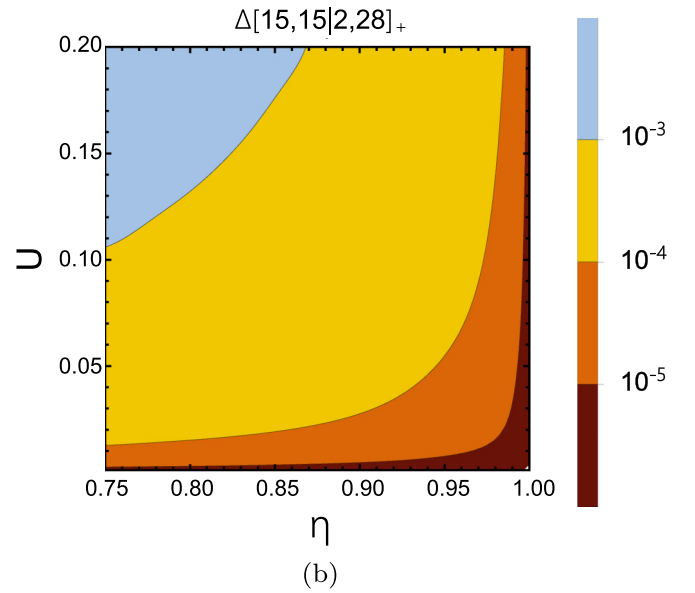
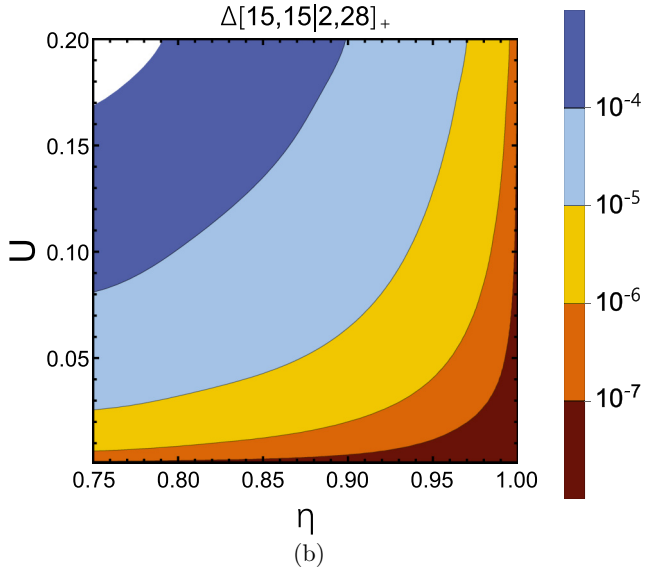
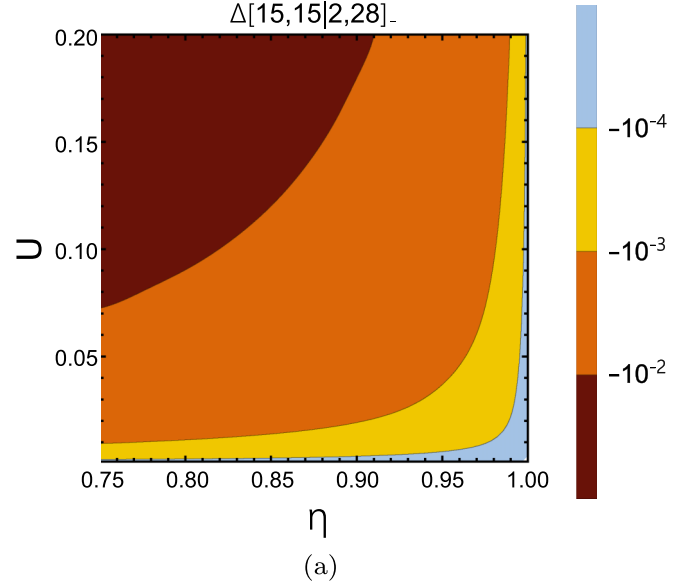
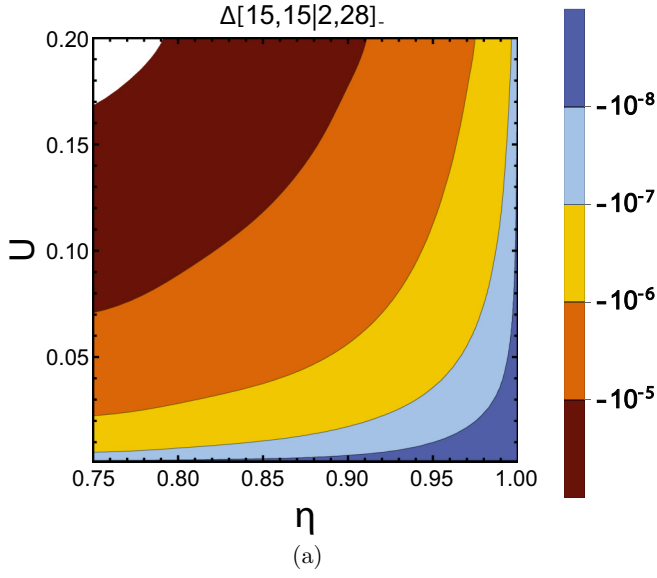


FIG. 7. The influence of U and η on the lower bound and upper bound. We plot the contour map of $\Delta_+[15, 15|2, 28]$ (a) and $\Delta_-[15, 15|2, 28]$ (b) when the transmittance of the beam splitter is $t = 0.407152$.

FIG. 8. The influence of U and η on the lower bound and upper bound with $S = 16$. Parts (a) and (b) are the contour maps of $\Delta_-(15, 15|2, 28)$ and $\Delta_+(15, 15|2, 28)$, respectively. In this simulation, we let $t = 0.407152$.

Therefore, for a particular detection outcome (k_1, k_2) , the probability $P_{k_1, k_2}^{\mu, \nu}$ given the input intensities μ, ν is

$$P_{k_1, k_2}^{\mu, \nu} = \frac{1}{4\pi^2} \int_0^{2\pi} \int_0^{2\pi} P_{k_1, k_2}^{\mu, \nu}(\phi_1, \phi_2) d\phi_1 d\phi_2, \quad (D6)$$

where

$$P_{k_1, k_2}^{\mu, \nu}(\phi_1, \phi_2) = \text{Tr}[(\hat{\Pi}_1 \otimes \hat{\Pi}_2) |\psi_{\mu'}\rangle\langle\psi_{\mu'}| \otimes |\psi_{\nu'}\rangle\langle\psi_{\nu'}|]. \quad (D7)$$

Following the method we proposed, if one has perfect PNR detectors showing that the detection efficiency is $\eta = 1$, one can have the theoretical conditional probabilities $P(k_1, k_2|j, K - j)$. For example, considering a Hong-Ou-Mandel dip for the conditional probabilities $P(3, 3|3, 3)$ and $P(5, 1|5, 1)$ at a beam splitter of transmittance $t = 1/2$ and

$5/6$, respectively, which has been studied in Ref. [34], the probabilities $P(3, 3|3, 3)$ and $P(5, 1|5, 1)$ as Fig. 6 shows can be written as

$$\begin{aligned} P(3, 3|3, 3) &= 0.3125 - 0.3125 \times 4^{-3\tau^2} + 0.5625 \times 4^{-2\tau^2} \\ &\quad - 0.5625 \times 4^{-\tau^2}, \\ P(5, 1|5, 1) &= 0.4019 - 0.4019 \times 4^{-\tau^2}. \end{aligned} \quad (D8)$$

It is obvious that these two theoretical curves are the same as those shown in Ref. [34].

APPENDIX E: THE ROBUSTNESS OF THE UPPER AND LOWER BOUNDS

To investigate how the choice of U and η affects the bounds, we plot the contour of $\Delta_+[15, 15|2, 28]$ and $\Delta_-[15, 15|2, 28]$ for example. As shown in Fig. 7, when U approaches 0 or η approaches 1, $\Delta_+[15, 15|2, 28]$ approaches 0. For a fixed value of U , the change of η has little influence on $\Delta_+[15, 15|2, 28]$. If we fix $U = 0.1$ for $0.80 \leq \eta \leq 0.92$, $\Delta_+[15, 15|2, 28]$ could be maintained around $O(10^{-5})$. This suggests that our method is quite robust to imperfections

of the detectors and the sources, given that they are well-characterized. It is worth mentioning that the robustness is important for experiments since both U and η have fluctuations that could potentially reduce the visibility.

In the case in which the TES resolves up to 16 photons, Fig. 8 shows the contour map of $\Delta(15, 15|2, 28)$ as a function of U and η . It is obvious that due to the lack of $\bar{B}_{16,15}^{\mu\nu}$ and $\bar{B}_{15,16}^{\mu\nu}$ to cancel out terms of 31-photon interference, both the upper bound and the lower bound (Δ_+, Δ_-) are increased compared to Fig. 7.

-
- [1] G. J. Pryde and A. G. White, *Phys. Rev. A* **68**, 052315 (2003).
- [2] H. Mikami, Y. Li, and T. Kobayashi, *Phys. Rev. A* **70**, 052308 (2004).
- [3] M. Reck, A. Zeilinger, H. J. Bernstein, and P. Bertani, *Phys. Rev. Lett.* **73**, 58 (1994).
- [4] A. Peruzzo, A. Laing, A. Politi, T. Rudolph, and J. L. O'Brien, *Nat. Commun.* **2**, 224 (2011).
- [5] E. Knill, R. Laflamme, and G. J. Milburn, *Nature (London)* **409**, 46 (2001).
- [6] R. Prevedel, P. Walther, F. Tiefenbacher, P. Böhi, R. Kaltenbaek, T. Jennewein, and A. Zeilinger, *Nature (London)* **445**, 65 (2007).
- [7] F. Xu, X. M. Zhang, H.-K. Lo, J.-W. Pan *et al.*, [arXiv:1903.09051](https://arxiv.org/abs/1903.09051).
- [8] M. A. Broome, A. Fedrizzi, S. Rahimi-Keshari, J. Dove, S. Aaronson, T. C. Ralph, and A. G. White, *Science* **339**, 794 (2013).
- [9] J. B. Spring, B. J. Metcalf, P. C. Humphreys, W. S. Kolthammer, X.-M. Jin, M. Barbieri, A. Datta, N. Thomas-Peter, N. K. Langford, D. Kundys, J. C. Gates, B. J. Smith, P. G. R. Smith, and I. A. Walmsley, *Science* **339**, 798 (2013).
- [10] M. Tillmann, B. Dakic, R. Heilmann, S. Nolte, A. Szameit, and P. Walther, *Nat. Photon.* **7**, 540 (2013).
- [11] A. Crespi, R. Osellame, R. Ramponi, D. J. Brod, E. F. Galvão, N. Spagnolo, C. Vitelli, E. Maiorino, P. Mataloni, and F. Sciarrino, *Nat. Photon.* **7**, 545 (2013).
- [12] H. Wang, Y. He, Y.-H. Li, Z.-E. Su, B. Li, H.-L. Huang, X. Ding, M.-C. Chen, C. Liu, J. Qin *et al.*, *Nat. Photon.* **11**, 361 (2017).
- [13] J. P. Dowling, *Contemp. Phys.* **49**, 125 (2008).
- [14] M. J. Holland and K. Burnett, *Phys. Rev. Lett.* **71**, 1355 (1993).
- [15] T. Nagata, R. Okamoto, J. L. O'Brien, K. Sasaki, and S. Takeuchi, *Science* **316**, 726 (2007).
- [16] I. Afek, O. Ambar, and Y. Silberberg, *Science* **328**, 879 (2010).
- [17] S. Rahimi-Keshari, M. A. Broome, R. Fickler, A. Fedrizzi, T. C. Ralph, and A. G. White, *Opt. Express* **21**, 13450 (2013).
- [18] H. K. Lo, M. Curty, and B. Qi, *Phys. Rev. Lett.* **108**, 130503 (2012).
- [19] H. Liu, W. Wang, K. Wei, X.-T. Fang, L. Li, N.-L. Liu, H. Liang, S.-J. Zhang, W. Zhang, H. Li *et al.*, *Phys. Rev. Lett.* **122**, 160501 (2019).
- [20] M. Lucamarini, Z. L. Yuan, J. F. Dynes, and A. J. Shields, *Nature (London)* **557**, 400 (2018).
- [21] C. K. Hong, Z. Y. Ou, and L. Mandel, *Phys. Rev. Lett.* **59**, 2044 (1987).
- [22] J.-W. Pan, Z.-B. Chen, C.-Y. Lu, H. Weinfurter, A. Zeilinger, and M. Żukowski, *Rev. Mod. Phys.* **84**, 777 (2012).
- [23] Z. Y. Ou, J.-K. Rhee, and L. J. Wang, *Phys. Rev. Lett.* **83**, 959 (1999).
- [24] B. H. Liu, F. W. Sun, Y. X. Gong, Y. F. Huang, G. C. Guo, and Z. Y. Ou, *Opt. Lett.* **32**, 1320 (2007).
- [25] X.-L. Niu, Y.-X. Gong, B.-H. Liu, Y.-F. Huang, G.-C. Guo, and Z. Y. Ou, *Opt. Lett.* **34**, 1297 (2009).
- [26] J. C. F. Matthews, A. Politi, D. Bonneau, and J. L. O'Brien, *Phys. Rev. Lett.* **107**, 163602 (2011).
- [27] G. Y. Xiang, Y. F. Huang, F. W. Sun, P. Zhang, Z. Y. Ou, and G. C. Guo, *Phys. Rev. Lett.* **97**, 023604 (2006).
- [28] X. Yuan, Z. Zhang, N. Lütkenhaus, and X. Ma, *Phys. Rev. A* **94**, 062305 (2016).
- [29] A. Aragonés, N. T. Islam, M. Eggleston, A. Lezama, J. Kim, and D. J. Gauthier, *Opt. Lett.* **43**, 3806 (2018).
- [30] P. Valente and A. Lezama, *J. Opt. Soc. Am. B* **34**, 924 (2017).
- [31] H. K. Lo, X. Ma, and K. Chen, *Phys. Rev. Lett.* **94**, 230504 (2005).
- [32] X. B. Wang, *Phys. Rev. Lett.* **94**, 230503 (2005).
- [33] T. Moroder, M. Curty, and N. Lütkenhaus, *New J. Phys.* **11**, 045008 (2009).
- [34] Á. Navarrete, W. Wang, F. Xu, and M. Curty, *New J. Phys.* **20**, 043018 (2018).
- [35] D. Fukuda, G. Fujii, T. Numata, K. Amemiya, A. Yoshizawa, H. Tsuchida, H. Fujino, H. Ishii, T. Itatani, S. Inoue, and T. Zama, *Opt. Express* **19**, 870 (2011).
- [36] L. Lolli, E. Taralli, and M. Rajteri, *J. Low Temp. Phys* **167**, 803 (2012).
- [37] Z. H. Levine, T. Gerrits, A. L. Migdall, D. V. Samarov, B. Calkins, A. E. Lita, and S. W. Nam, *J. Opt. Soc. Am. B* **29**, 2066 (2012).
- [38] A. E. Lita, A. J. Miller, and S. W. Nam, *Opt. Express* **16**, 3032 (2008).
- [39] J. Sperling, W. R. Clements, A. Eckstein, M. Moore, J. J. Renema, W. S. Kolthammer, S. W. Nam, A. Lita, T. Gerrits, W. Vogel, G. S. Agarwal, and I. A. Walmsley, *Phys. Rev. Lett.* **118**, 163602 (2017).
- [40] H. Oruç and H. K. Akmaz, *J. Comput. Appl. Math.* **172**, 49 (2004).